Chapter 1

Seismic Wave Propagation with General Gate-based Quantum Computing

Hoang Anh Nguyen

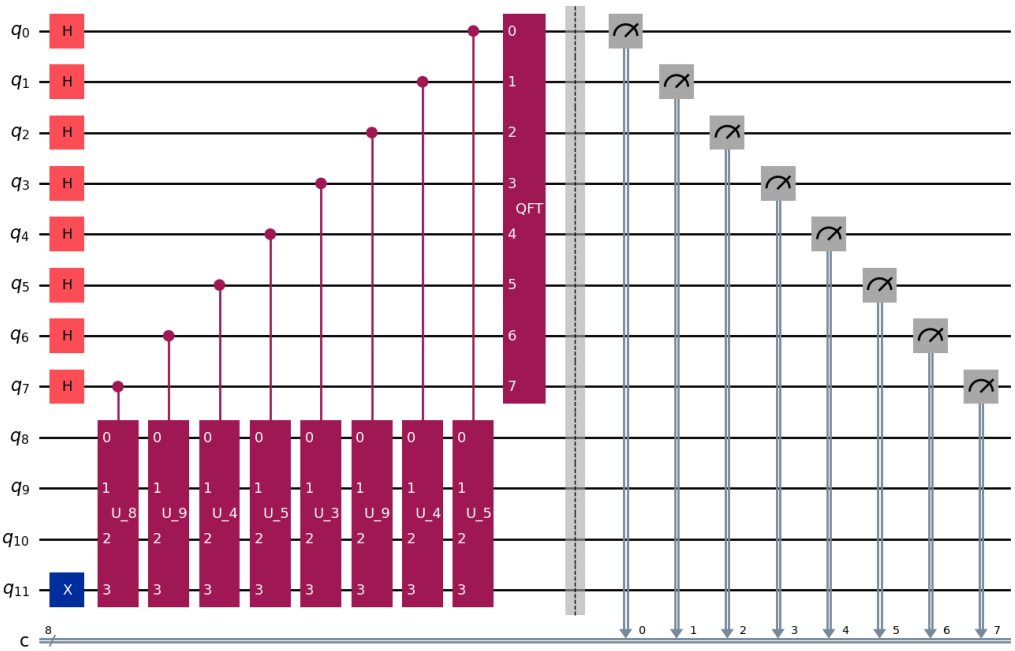

Summary

Project Goals

- Study the wave propagation using general gate-based quantum computing.
- Replicate the study conducted by Yuki et al, Hamiltonian simulation for hyperbolic partial differential equations by scalable quantum circuits, applying their methodologies and analyses to validate findings and explore implications.

Data

The synthetic data

Introduction

Gate-based Quantum Computing

Quantum computing leverages principles of quantum mechanics, notably superposition and entanglement, to solve certain computational problems significantly faster than classical computing. Among various quantum computational paradigms, gate-based quantum computing represents the most widely adopted model. It operates by manipulating quantum states through quantum gates, analogous to classical logic gates, but distinctly different due to their inherent quantum mechanical nature Nielsen and Chuang (2010).

The fundamental building block of quantum computing is the quantum bit, or qubit. Unlike classical bits, qubits exist in a superposition of two basis states. A single qubit exists in a superposition state described by

$$|\psi\rangle = \alpha|0\rangle + \beta|1\rangle,$$

where $\alpha, \beta \in \mathbb{C}$ and $|\alpha|^2 + |\beta|^2 = 1$. An n-qubit system spans a 2^n-dimensional complex Hilbert space, allowing it to represent a superposition over 2^n classical states This superposition principle also allows quantum computers to process a vast number of possibilities simultaneously. Quantum algorithms such as Grover's algorithm Grover (1996), Shor's algorithm Shor (1997), and the Harrow-Hassidim-Lloyd (HHL) algorithm Dervovic et al. (2018) illustrate the computational advantages of gate-based quantum computing. Grover's algorithm offers a quadratic speedup for unstructured search problems, reducing the complexity from $O(N)$ in classical brute-force approaches to $O(\sqrt{N})$. Shor's algorithm provides an exponential speedup for integer factorization, solving the problem in polynomial time compared to the best-known classical sub-exponential methods. The HHL algorithm enables efficient solutions to certain linear systems of equations, achieving an exponential speedup in specific cases by solving a system of size N in time $O(\log N)$, under the assumption of a well-conditioned and sparse matrix.

Quantum Gates & Circuits

This part reviews the quantum computing gate, for more information, we recommend to read the book of Nielsen and Chuang (2010). Quantum gates manipulate qubits by applying unitary transformations. Mathematically, a quantum gate U acting on a state $|\psi\rangle$ transforms it as:

$$|\psi'\rangle = U|\psi\rangle, \quad \text{where } U^\dagger U = UU^\dagger = I$$

This ensures the evolution is reversible and norm-preserving, a key property in quantum mechanics. Quantum gate-based computing mimics the classical computing paradigm, where computations are performed by applying logic gates (such as AND, OR, and NOT) to bits. Similarly, quantum computing performs operations on qubits using quantum gates. However, unlike classical logic gates, quantum gates are reversible and represented by unitary matrices, allowing a much richer set of operations. Quantum computers support not only basic logic but also phase shifts, entanglement, and superposition through a diverse collection of gates, far beyond those found in classical circuits.

Single-Qubit Gates

Here is the example of some frequently used gates.

- Pauli Gates (X, Y, Z): these gates correspond to the Pauli matrices and represent fundamental quantum operations.

$$X = \sigma_x = \begin{pmatrix} 0 & 1 \\ 1 & 0 \end{pmatrix}, \qquad X|0\rangle = |1\rangle, \quad X|1\rangle = |0\rangle$$
$$Y = \sigma_y = \begin{pmatrix} 0 & -i \\ i & 0 \end{pmatrix},$$
$$Z = \sigma_z = \begin{pmatrix} 1 & 0 \\ 0 & -1 \end{pmatrix}$$

  X: Analogous to a classical NOT gate, flips the qubit. Y, Z: Introduce phase shifts and complex amplitude transformations.

- Hadamard Gate (H): this is one of the most important component almost quantum algorithm because it creates equal superpositions of the basis states:

$$H = \frac{1}{\sqrt{2}} \begin{pmatrix} 1 & 1 \\ 1 & -1 \end{pmatrix}, \quad H|0\rangle = \frac{|0\rangle + |1\rangle}{\sqrt{2}}, \quad H|1\rangle = \frac{|0\rangle - |1\rangle}{\sqrt{2}}$$

  Used extensively in quantum algorithms to create superpositions (e.g., Grover's and Shor's algorithms).

- Phase Gates (S, T): These gates introduce relative phases between basis states.

$$S = \begin{pmatrix} 1 & 0 \\ 0 & i \end{pmatrix}, \quad T = \begin{pmatrix} 1 & 0 \\ 0 & e^{i\pi/4} \end{pmatrix}$$

  S: Applies a phase of i to $|1\rangle$. T: Applies a smaller phase, useful for finer quantum phase control.

Multi-Qubit Gates

- CNOT Gate (Controlled-NOT):

  A two-qubit gate that flips the target qubit if the control qubit is $|1\rangle$. The matrix form is:

$$\text{CNOT} = \begin{pmatrix} 1 & 0 & 0 & 0 \\ 0 & 1 & 0 & 0 \\ 0 & 0 & 0 & 1 \\ 0 & 0 & 1 & 0 \end{pmatrix}$$

Its action on computational basis states is:

$$\text{CNOT}|00\rangle = |00\rangle, \quad \text{CNOT}|01\rangle = |01\rangle, \quad \text{CNOT}|10\rangle = |11\rangle, \quad \text{CNOT}|11\rangle = |10\rangle$$

It is the primary entangling gate in quantum circuits.

- Toffoli Gate (CCNOT):

  A three-qubit gate that flips the target qubit only when both control qubits are $|1\rangle$. Its matrix is:

$$\text{CCNOT} = \begin{pmatrix} 1 & 0 & 0 & 0 & 0 & 0 & 0 & 0 \\ 0 & 1 & 0 & 0 & 0 & 0 & 0 & 0 \\ 0 & 0 & 1 & 0 & 0 & 0 & 0 & 0 \\ 0 & 0 & 0 & 1 & 0 & 0 & 0 & 0 \\ 0 & 0 & 0 & 0 & 1 & 0 & 0 & 0 \\ 0 & 0 & 0 & 0 & 0 & 1 & 0 & 0 \\ 0 & 0 & 0 & 0 & 0 & 0 & 0 & 1 \\ 0 & 0 & 0 & 0 & 0 & 0 & 1 & 0 \end{pmatrix}$$

  It is universal for classical computation when embedded in a quantum circuit and essential for reversible logic.

Note that quantum gates are mathematically represented as matrices acting on complex vector spaces. This means that, in principle, the behavior of quantum circuits can be simulated on classical computers using matrix multiplication and linear algebra techniques. However, such simulations are computationally expensive, as the state vector of an n-qubit system has 2^n complex amplitudes, making the simulation cost grow exponentially with the number of qubits.

Quantum Circuits and Measurement

A quantum computation is executed through a sequence of quantum gates arranged in a quantum circuit. Mathematically, a quantum circuit corresponds to a unitary transformation composed of multiple gate operations:

$$U_{\text{circuit}} = U_k U_{k-1} \cdots U_2 U_1$$

Applying this circuit to an initial quantum state $|\psi_{\text{init}}\rangle$ yields the final quantum state:

$$|\psi_{\text{final}}\rangle = U_{\text{circuit}}|\psi_{\text{init}}\rangle$$

To extract classical information from a quantum state, we perform a measurement. Measurement collapses the final quantum state into a classical bitstring outcome, according to the Born rule. The probability of observing a particular outcome x is given by:

$$P(x) = |\langle x|\psi_{\text{final}}\rangle|^2$$

This probabilistic nature of quantum measurement is a fundamental distinction from deterministic classical computation. The example of the quantum period finding algorithm that used as a part in the Shor's algorithm is presented in the Fig. 1.1 Shor (1997). Measurement is a fundamental operation in quantum computing that extracts classical information from a quantum system. Unlike classical systems, which can be observed without altering their state, quantum systems collapse into specific basis states upon measurement. This irreversible process is governed by the Born rule Nielsen and Chuang (2010).

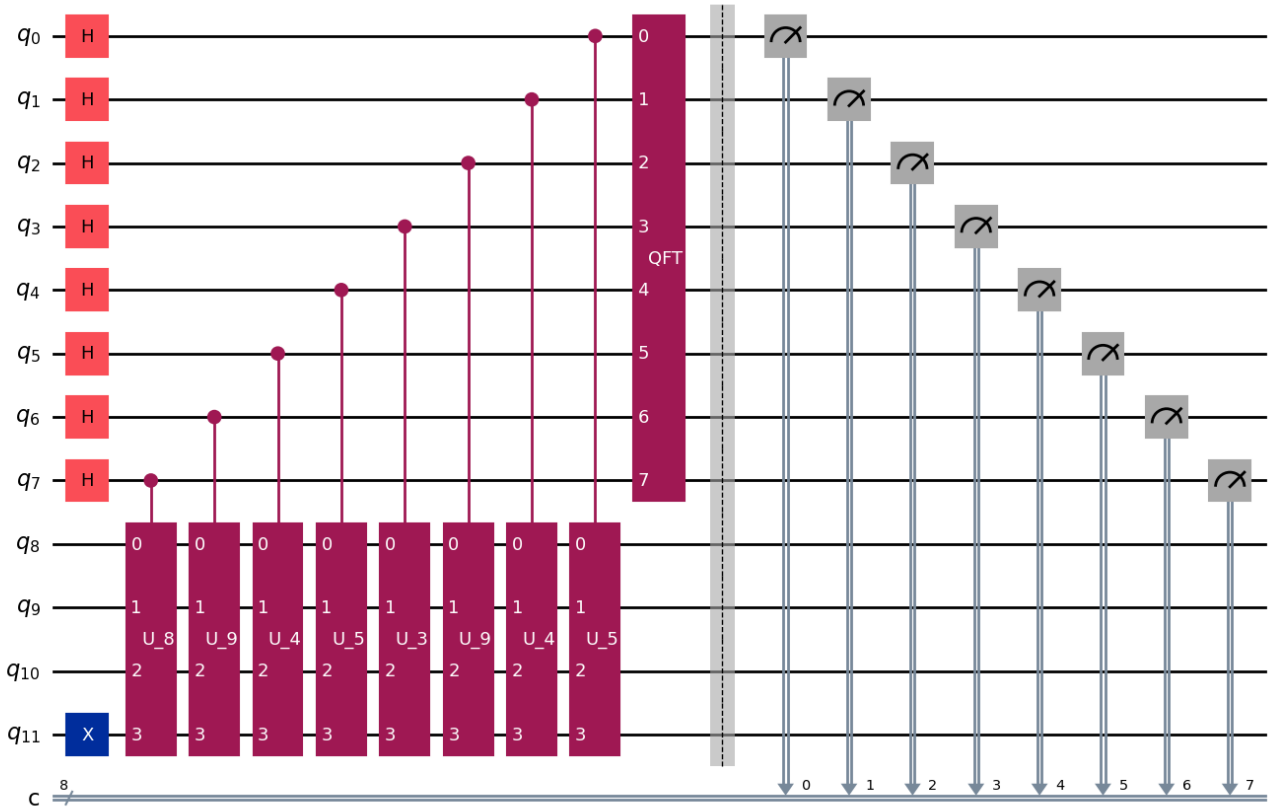

Figure 1.1: Quantum circuit for period finding, a subroutine in Shor's algorithm. The top 8 qubits (q_0 to q_7) serve as the control register initialized in superposition using Hadamard gates H. The bottom 4 qubits (q_8 to q_{11}) are initialized with the state $|1\rangle$, where the X gate applies this to q_{11}. Controlled unitary operations U^x encode the periodic function $f(x) = a^x \bmod N$. The inverse Quantum Fourier Transform (QFT) is applied to the control register to extract the period, followed by measurements in the computational basis. The classical register c stores the measurement outcomes. The circuit is simulated using qiskit Javadi-Abhari et al. (2024).

Hamiltonian

In geophysics, wave propagation through the Earth's subsurface is typically modeled by partial differential equations (PDEs), such as the acoustic or elastic wave equations. These PDEs describe how seismic waves travel through heterogeneous media, revealing subsurface structures based on variations in wave speed, density, and material properties. Traditional numerical methods, such as finite-difference or finite-element solvers, discretize these PDEs to simulate wavefields, which are then used for imaging and inversion tasks.

To transition from classical PDE-based modeling to quantum simulation, one must reformulate the underlying equations into a Hamiltonian framework suitable for quantum computing. This involves discretizing the wave equation in space and encoding the resulting differential operator as a matrix A, which captures the physical dynamics of the medium—such as velocity contrasts, anisotropy, and boundary conditions. To ensure that the evolution is unitary, as required in quantum mechanics, we construct a Hermitian matrix $\mathcal{H}_A$ as follows:

$$\mathcal{H}_A = \begin{pmatrix} 0 & A \\ A^\dagger & 0 \end{pmatrix}.$$

This structure guarantees that $\mathcal{H}_A$ is Hermitian. Consequently, the matrix exponential $e^{-i\mathcal{H}_A t}$ defines a unitary operator that evolves the quantum state over time. This quantum evolution mimics the propagation of seismic wavefields in the Earth and can be implemented as a gate sequence in quantum circuits.

By encoding geophysical wave physics into a Hermitian Hamiltonian, we enable quantum computers to simulate seismic wave propagation efficiently, with the potential to outperform classical solvers in high-resolution, high-dimensional models. The Hamiltonian in quantum mechanics is a central operator that represents the total energy of a quantum system. It encompasses both kinetic and potential energy and governs the system's time evolution. Mathematically, the Hamiltonian is denoted by the Hermitian operator $\hat{\mathcal{H}}$, and its action on a quantum state $|\psi(t)\rangle$ is described by the time-dependent Schrödinger equation:

$$i\hbar\frac{\partial}{\partial t}|\psi(t)\rangle = \hat{\mathcal{H}}|\psi(t)\rangle$$

Here, $\hbar$ is the reduced Planck constant, and $|\psi(t)\rangle$ is the state vector of the system at time t. The eigenvalues of $\hat{\mathcal{H}}$ correspond to the possible energy levels of the system, and its eigenvectors represent the stationary states. In finite-dimensional quantum systems, $\hat{\mathcal{H}}$ can be expressed as a Hermitian matrix whose spectral decomposition provides a complete basis of energy eigenstates.

Lemma. Let $A \in \mathbb{C}^{N\times N}$ be a complex-valued matrix. Define the block matrix

$$\mathcal{H}_A = \begin{pmatrix} 0 & A \\ A^\dagger & 0 \end{pmatrix}.$$

Then $\mathcal{H}_A$ is Hermitian and the matrix exponential $e^{-i\mathcal{H}_A t}$ is unitary for all real t, and can therefore be used as a valid gate or a set of gate in quantum computing.

Proof. We compute the conjugate transpose:

$$\mathcal{H}_A^\dagger = \left(\begin{pmatrix} 0 & A \\ A^\dagger & 0 \end{pmatrix}\right)^\dagger = \begin{pmatrix} 0 & A \\ A^\dagger & 0 \end{pmatrix} = \mathcal{H}_A.$$

So $\mathcal{H}_A$ is Hermitian. By standard results, if $\mathcal{H}$ is Hermitian, then $e^{-i\mathcal{H}t}$ is unitary:

$$(e^{-i\mathcal{H}t})^\dagger = e^{i\mathcal{H}t}, \quad e^{i\mathcal{H}t}e^{-i\mathcal{H}t} = I.$$

Thus $e^{-i\mathcal{H}_A t}$ is unitary, suitable as a gate in quantum computing. A standard result in linear algebra and quantum mechanics is: If $\mathcal{H}$ is Hermitian, then $U(t) = e^{-i\mathcal{H}t}$ is a unitary matrix for all real t. To verify unitarity, we check that

$$U(t)^\dagger = \left(e^{-i\mathcal{H}t}\right)^\dagger = e^{i\mathcal{H}^\dagger t}.$$

Since $\mathcal{H}$ is Hermitian, $\mathcal{H}^\dagger = \mathcal{H}$, so

$$U(t)^\dagger = e^{i\mathcal{H}t} \quad \Rightarrow \quad U(t)^\dagger U(t) = e^{i\mathcal{H}t}e^{-i\mathcal{H}t} = e^0 = I.$$

Therefore, $U(t)$ is unitary. Applying this to our matrix $\mathcal{H}_A$, which is Hermitian, it follows that $e^{-i\mathcal{H}_A t}$ is unitary. A quantum computer can be treated as an unitary gate unitary acting on a finite-dimensional state space, followed by a measurement 1.2. So we can simulate a quantum circuit by explicitly multiplying the unitary matrices and then sampling measurement outcomes.

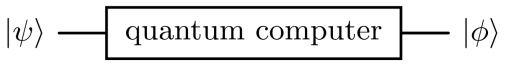

Figure 1.2: Quantum computer as an unitary gate.

Hamiltonian Formulation from the Acoustic Wave Equation

The acoustic wave equation governs pressure wave propagation in a compressible medium and is given by the second-order partial differential equation:

$$\frac{\partial^2 u(t,\mathbf{x})}{\partial t^2} = c^2 \nabla^2 u(t,\mathbf{x}),$$

where $u(t,\mathbf{x})$ denotes the scalar pressure field, c is the wave speed, and ∇^2 is the Laplacian operator acting on the spatial coordinates $\mathbf{x} \in \mathbb{R}^d$.

To transform this into a first order in time system which is suitable for Hamiltonian or quantum like formulation, we introduce an augmented state vector $\boldsymbol{\psi}(t,\mathbf{x})$ that combines the pressure field and its derivatives. This allows the wave equation to be recast into a Schrödinger-type equation with $\mathcal{H}$ is a Hermitian operator that acts as a Hamiltonian governing time evolution:

$$\frac{\partial \boldsymbol{\psi}(t,\mathbf{x})}{\partial t} = -i\mathcal{H}\boldsymbol{\psi}(t,\mathbf{x}),$$

Case $d = 1$: 1D Acoustic Wave Equation, let:

$$\boldsymbol{\psi}(t,x_1) = \begin{pmatrix} \frac{\partial u(t,x_1)}{\partial t} \\ ic\frac{\partial u(t,x_1)}{\partial x_1} \end{pmatrix}, \quad \mathcal{H} = c\begin{pmatrix} 0 & \frac{\partial}{\partial x_1} \\ -\frac{\partial}{\partial x_1} & 0 \end{pmatrix}.$$

Case $d = 2$: 2D Acoustic Wave Equation, for two spatial dimensions, the wave equation is:

$$\frac{\partial^2 u(t,\mathbf{x})}{\partial t^2} = c^2\left(\frac{\partial^2 u}{\partial x_1^2} + \frac{\partial^2 u}{\partial x_2^2}\right).$$

We now define the state vector and Hamiltonian as:

$$\boldsymbol{\psi}(t,\mathbf{x}) = \begin{pmatrix} \frac{\partial u(t,\mathbf{x})}{\partial t} \\ ic\left(\frac{\partial u(t,\mathbf{x})}{\partial x_1} + i\frac{\partial u(t,\mathbf{x})}{\partial x_2}\right) \end{pmatrix}, \quad \mathcal{H} = c\begin{pmatrix} 0 & \frac{\partial}{\partial x_1} - i\frac{\partial}{\partial x_2} \\ -\frac{\partial}{\partial x_1} - i\frac{\partial}{\partial x_2} & 0 \end{pmatrix}.$$

The operator $\mathcal{H}$ is Hermitian, ensuring unitary time evolution. In both case of 1D and 2D Acoustic wave equation, we have:

$$\frac{\partial \boldsymbol{\psi}(t,\mathbf{x})}{\partial t} = -i\mathcal{H}\boldsymbol{\psi}(t,\mathbf{x})$$

provides a natural connection to Hamiltonian simulation on quantum computers recovering the original second-order wave equation, where $\mathcal{H}$ can be discretized and encoded as a matrix acting on a quantum register. The proofs are shown in the Appendix section.

The next essential step in simulating quantum dynamics is to map the continuous-time evolution governed by the Schrödinger equation into a discrete quantum circuit composed of quantum gates. Specifically, this involves expressing the Hamiltonian H of the system in a form that can be implemented using standard gate-based quantum computing operations. We recommend referring to the detailed derivation and construction in the work by Sato et al. (2024), which provides a thorough approach to this decomposition. The quantum circuit representation of the time evolution operator V, which corresponds to e^{-iHt}, is shown in Figure 1.3. In this figure, the operator V is constructed as a sequence of local unitary operations W_j, each acting on a subset of qubits. The idea is to decompose the global unitary evolution into a product of smaller unitaries, where each W_j approximates the evolution due to a local term in the Hamiltonian.

The subcircuit implementing W_j is further decomposed into basic quantum gates using controlled operations and single-qubit gates such as H (Hadamard), RZ (rotation around the Z-axis), and phase gates P and $P^\dagger$. These operations are conditioned on the states of multiple qubits, ensuring that the dynamics respect the structure of the Hamiltonian, particularly in

systems governed by nearest-neighbor or spatially structured interactions. The circuit in Figure 1.3 illustrates a modular approach to Hamiltonian simulation, where the full operator V is built from repeated applications of gate blocks W_j, enabling scalable and efficient quantum simulation of time evolution.

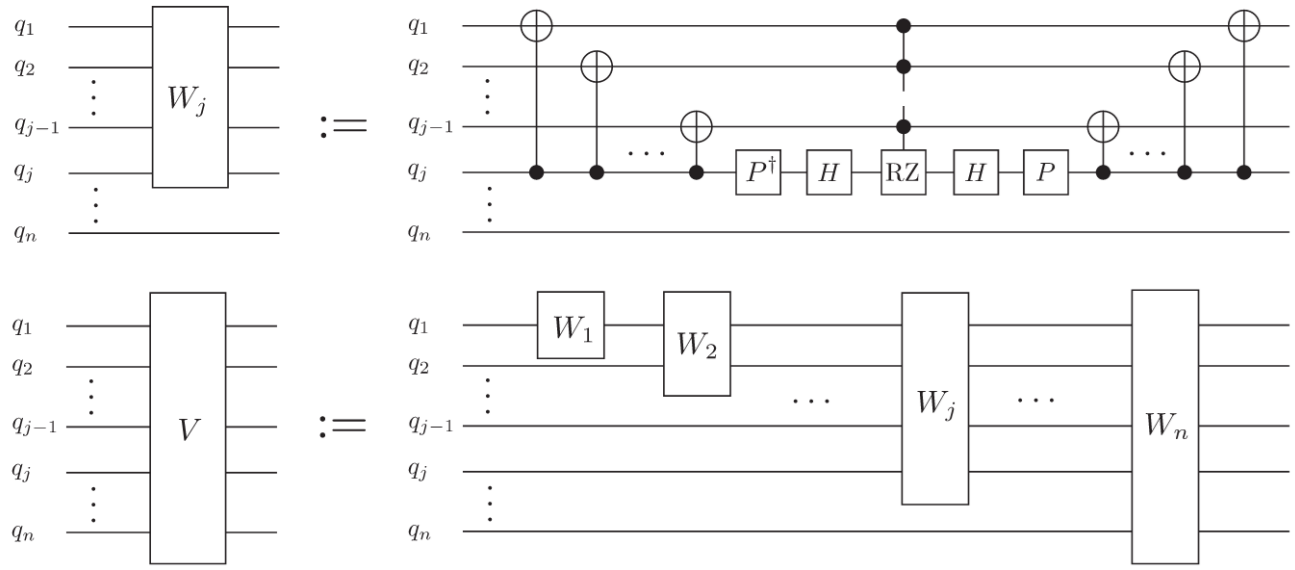

Figure 1.3: Quantum circuit to implement the time evolution operator V Sato et al. (2024)

Results

To initialize the quantum simulation, we translate the classical initial conditions of the wave equation into a quantum state. We assume the classical displacement field $u(t, x_{j_1}, x_{j_2})$ is initially zero throughout the domain:

$$u(0, x_{j_1}, x_{j_2}) = 0,$$

but its time derivative is nonzero over a centered region:

$$\left.\frac{\partial u(t, x_{j_1}, x_{j_2})}{\partial t}\right|_{t=0} = \begin{cases} 1 & \text{if } 2^{n-2} \leq x_{j_1}, x_{j_2} < 2^{n-1}, \\ 0 & \text{otherwise.} \end{cases}$$

We encode this initial velocity perturbation into a quantum state as follows. The wavefunction at $t = 0$ is constructed as a uniform superposition over the indices j_1 and j_2 in the active region:

$$|\psi(0)\rangle = |0\rangle \otimes \frac{1}{2^{n-2}} \sum_{j_1=0}^{2^{n-2}-1} \sum_{j_2=0}^{2^{n-2}-1} |0\rangle|1\rangle|j_1\rangle \otimes |0\rangle|1\rangle|j_2\rangle,$$

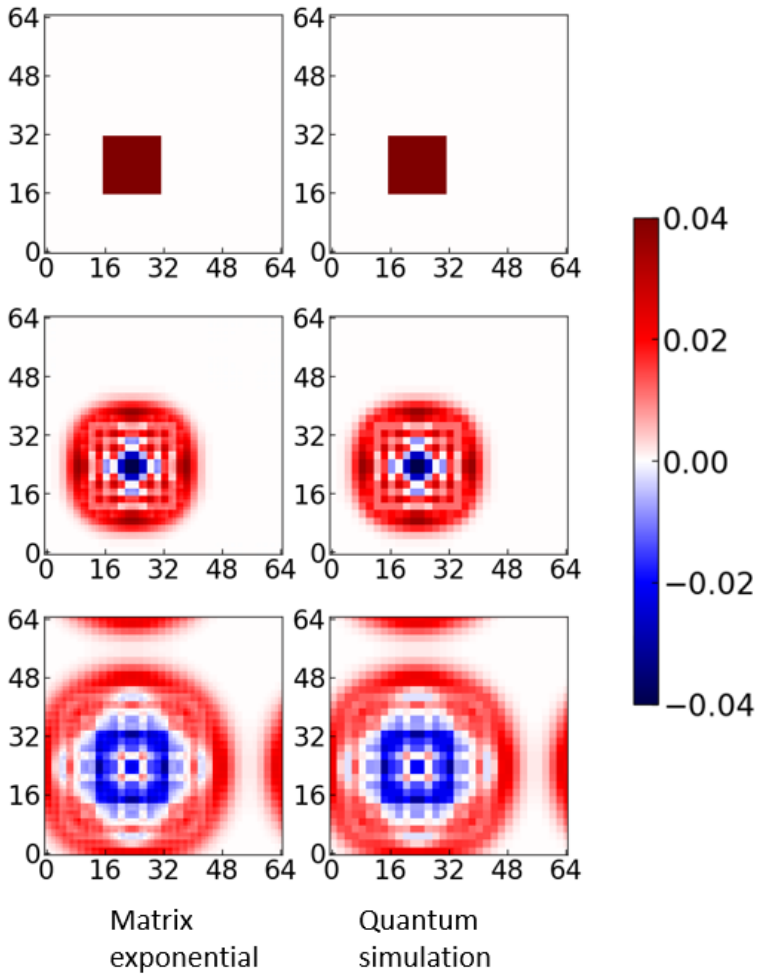

Figure 1.4: The results of running the isotropic acoustic wave equation. The left and the right figure is the wave equation solving by matrix exponential and the quantum gate simulation, respectively. Note that there is no measurement in the circuit.

where the binary registers $|j_1\rangle$ and $|j_2\rangle$ represent spatial coordinates, and the ancillary qubits encode initial momentum along those directions. The full state thus reflects the finite-support nature of the initial time derivative in the classical field.

Figure 1.4 presents the results obtained from both the matrix exponential method and a quantum circuit simulator for solving the acoustic wave equation under a constant velocity model at different time. Periodic boundary conditions are applied to emulate an infinite domain. In this simulation, the total spatial grid size is $64 \times 64 = 4096$, which is mapped onto a quantum register using a total of 13 qubits. Specifically, 12 of these qubits are used to represent the discretized wavefield, while the remaining qubit acts as an ancillary qubit to facilitate operations related to the spatial derivative operator.

The wave equation is reformulated into a first-order differential equation resembling the time-dependent Schrödinger equation, $\frac{\partial \psi(t,\mathbf{x})}{\partial t} = -i\mathcal{H}\psi(t,\mathbf{x})$, where $\mathcal{H}$ is the effective Hamiltonian operator (matrix) that governs the system's dynamics. The solution to this

equation is given by a unitary evolution $\psi(t, \mathbf{x}) = e^{-i\mathcal{H}t}\psi(0, \mathbf{x})$, and is naturally suited to implementation on a quantum computer, as such unitary evolutions can be decomposed into quantum gates.

This formulation demonstrates a key advantage of quantum computation: the ability to evolve a high-dimensional wavefield using only a logarithmic number of qubits relative to the grid size. Even with just 13 qubits, the simulation can handle 4096 spatial points, showcasing the exponential memory compression offered by quantum systems. These results serve as a proof-of-concept that quantum wave solvers can offer scalable and memory-efficient alternatives to classical numerical methods in geophysical modeling and related applications.

Conclusion

In this chapter, we investigated the feasibility and methodology of using gate-based quantum computing to simulate seismic wave propagation governed by the acoustic wave equation. We began by translating the classical second-order partial differential equation into a first-order Schrödinger-type formulation, allowing it to be naturally expressed in terms of a Hermitian Hamiltonian operator. This reformulation made it possible to implement wavefield evolution as a unitary matrix exponential e^{-iHt}, consistent with the rules of quantum mechanics. We detailed how the Hamiltonian was constructed from finite-difference approximations and encoded into a block structure to ensure Hermiticity. The resulting operator was implemented using quantum circuits, where the time evolution operator V was decomposed into smaller local gates W_j, facilitating scalable circuit construction. The encoding of initial conditions into a quantum register enabled simulation of a 2D wavefield using only 13 qubits, demonstrating an exponential compression in memory compared to classical grid-based methods. The numerical results, based on both classical matrix exponentials and quantum gate simulators, confirmed the correctness of this approach in a constant velocity medium with periodic boundary conditions. The successful simulation of a 64 × 64 grid using quantum resources provides a compelling proof-of-concept for leveraging quantum computation in seismic modeling applications.

Building upon the foundation established in this study, several promising directions exist for future development. One immediate extension involves the injection of seismic sources into the quantum-simulated model. Introducing source terms allows for more realistic simulations of wave propagation scenarios, enabling studies of source-receiver configurations, energy distributions, and waveform characteristics. Next, expanding the wave solver to support heterogeneous velocity models is crucial. While this work assumes a constant velocity for simplicity and demonstration purposes, real-world geophysical applications require accurate handling of spatial variations in wave speed. A particularly impactful avenue is the integration of quantum-enhanced Full Waveform Inversion (FWI) into the simulation pipeline. By using adjoint-state methods or data-driven gradients in conjunction with quantum-forward modeled data, this approach could offer a novel strategy for updating velocity models more efficiently than classical FWI. Quantum circuits could be used to perform forward and possibly adjoint simulations in parallel, with potential benefits in both speed and memory efficiency. The incorporation of a Quantum Hybrid Neural Network (QHNN) presents a powerful opportunity

to bridge classical deep learning and quantum simulation. Such a hybrid framework can be used to learn mappings between observed data and model parameters, accelerate inversion convergence, or denoise quantum outputs through learned priors. These QHNNs can be trained classically while embedding quantum layers for parts of the physics, enabling quantum-classical synergy. By fusing neural architectures with quantum operations, future workflows may yield both physically interpretable and computationally superior solutions for seismic imaging and inversion.

Appendix

Proof that the first-Order Hamiltonian formulation recovers the wave equation in one dimension 1D

From the definition of the state vector:

$$\boldsymbol{\psi}(t,x_1) = \begin{pmatrix} \psi_1(t,x_1) \\ \psi_2(t,x_1) \end{pmatrix} = \begin{pmatrix} \frac{\partial u(t,x_1)}{\partial t} \\ ic\frac{\partial u(t,x_1)}{\partial x_1} \end{pmatrix},$$

and the Hamiltonian operator:

$$\mathcal{H} = c\begin{pmatrix} 0 & \frac{\partial}{\partial x_1} \\ -\frac{\partial}{\partial x_1} & 0 \end{pmatrix},$$

we write the first-order system:

$$\frac{\partial}{\partial t}\begin{pmatrix} \psi_1 \\ \psi_2 \end{pmatrix} = -i\mathcal{H}\begin{pmatrix} \psi_1 \\ \psi_2 \end{pmatrix} = -ic\begin{pmatrix} 0 & \frac{\partial}{\partial x_1} \\ -\frac{\partial}{\partial x_1} & 0 \end{pmatrix}\begin{pmatrix} \psi_1 \\ \psi_2 \end{pmatrix} = -ic\begin{pmatrix} \frac{\partial \psi_2}{\partial x_1} \\ -\frac{\partial \psi_1}{\partial x_1} \end{pmatrix}.$$

Equating components, we obtain:

$$\frac{\partial \psi_1}{\partial t} = -ic\frac{\partial \psi_2}{\partial x_1}, \qquad \frac{\partial \psi_2}{\partial t} = ic\frac{\partial \psi_1}{\partial x_1}.$$

Substitute the definition $\psi_1 = \partial_t u$, and compute its time derivative:

$$\frac{\partial^2 u}{\partial t^2} = \frac{\partial \psi_1}{\partial t} = -ic\frac{\partial \psi_2}{\partial x_1}.$$

Now substitute $\psi_2 = ic\partial_{x_1} u$:

$$\frac{\partial \psi_2}{\partial x_1} = ic\frac{\partial^2 u}{\partial x_1^2}, \quad \Rightarrow \quad \frac{\partial^2 u}{\partial t^2} = -ic \cdot ic\frac{\partial^2 u}{\partial x_1^2} = c^2\frac{\partial^2 u}{\partial x_1^2}.$$

This is exactly the original second-order acoustic wave equation in 1D:

$$\frac{\partial^2 u}{\partial t^2} = c^2\frac{\partial^2 u}{\partial x_1^2}.$$

Hence, the first-order Schrödinger-type equation with the defined Hamiltonian $\mathcal{H}$ recovers the classical wave dynamics.

Proof that the first-Order Hamiltonian formulation recovers the wave equation in two dimensions (2D)

We now show that the corrected 2D Hamiltonian form recovers the standard acoustic wave equation:

$$\frac{\partial^2 u}{\partial t^2} = c^2 \left(\frac{\partial^2 u}{\partial x_1^2} + \frac{\partial^2 u}{\partial x_2^2} \right).$$

Let the augmented state vector be:

$$\boldsymbol{\psi}(t, \mathbf{x}) = \begin{pmatrix} \psi_1(t, \mathbf{x}) \\ \psi_2(t, \mathbf{x}) \end{pmatrix} = \begin{pmatrix} \frac{\partial u(t,\mathbf{x})}{\partial t} \\ ic \left(\frac{\partial u(t,\mathbf{x})}{\partial x_1} + i \frac{\partial u(t,\mathbf{x})}{\partial x_2} \right) \end{pmatrix},$$

and let the Hamiltonian operator be defined as:

$$\mathcal{H} = c \begin{pmatrix} 0 & \partial_{x_1} - i\partial_{x_2} \\ -\partial_{x_1} - i\partial_{x_2} & 0 \end{pmatrix}.$$

The evolution equation is:

$$\frac{\partial}{\partial t} \begin{pmatrix} \psi_1 \\ \psi_2 \end{pmatrix} = -i\mathcal{H} \begin{pmatrix} \psi_1 \\ \psi_2 \end{pmatrix} = -ic \begin{pmatrix} (\partial_{x_1} - i\partial_{x_2})\psi_2 \\ -(\partial_{x_1} + i\partial_{x_2})\psi_1 \end{pmatrix}.$$

From the first component:

$$\frac{\partial \psi_1}{\partial t} = -ic(\partial_{x_1} - i\partial_{x_2})\psi_2.$$

Now substitute:

$$\psi_2 = ic \left(\frac{\partial u}{\partial x_1} + i \frac{\partial u}{\partial x_2} \right).$$

Compute the derivative:

$$(\partial_{x_1} - i\partial_{x_2})\psi_2 = (\partial_{x_1} - i\partial_{x_2}) \left[ic \left(\frac{\partial u}{\partial x_1} + i \frac{\partial u}{\partial x_2} \right) \right] = ic(\partial_{x_1} - i\partial_{x_2}) \left(\frac{\partial u}{\partial x_1} + i \frac{\partial u}{\partial x_2} \right).$$

Using distributivity and product of operators:

$$= ic \left(\frac{\partial^2 u}{\partial x_1^2} + i \frac{\partial^2 u}{\partial x_1 \partial x_2} - i \frac{\partial^2 u}{\partial x_2 \partial x_1} - i^2 \frac{\partial^2 u}{\partial x_2^2} \right) = ic \left(\frac{\partial^2 u}{\partial x_1^2} + \frac{\partial^2 u}{\partial x_2^2} \right).$$

Then:

$$\frac{\partial \psi_1}{\partial t} = -ic \cdot ic \left(\frac{\partial^2 u}{\partial x_1^2} + \frac{\partial^2 u}{\partial x_2^2} \right) = c^2 \left(\frac{\partial^2 u}{\partial x_1^2} + \frac{\partial^2 u}{\partial x_2^2} \right).$$

Since $\psi_1 = \partial_t u$, we conclude:

$$\frac{\partial^2 u}{\partial t^2} = c^2 \left(\frac{\partial^2 u}{\partial x_1^2} + \frac{\partial^2 u}{\partial x_2^2} \right),$$

which confirms that the corrected Hamiltonian recovers the classical 2D acoustic wave equation.

Bibliography

Dervovic, D., M. Herbster, P. Mountney, S. Severini, N. Usher, and L. Wossnig, 2018, Quantum linear systems algorithms: a primer.

Grover, L. K., 1996, A fast quantum mechanical algorithm for database search.

Javadi-Abhari, A., M. Treinish, K. Krsulich, C. J. Wood, J. Lishman, J. Gacon, S. Martiel, P. D. Nation, L. S. Bishop, A. W. Cross, B. R. Johnson, and J. M. Gambetta, 2024, Quantum computing with Qiskit.

Nielsen, M. A., and I. L. Chuang, 2010, Quantum computation and quantum information: 10th anniversary edition: Cambridge University Press.

Sato, Y., R. Kondo, I. Hamamura, T. Onodera, and N. Yamamoto, 2024, Hamiltonian simulation for hyperbolic partial differential equations by scalable quantum circuits: Phys. Rev. Res., **6**, no. 3, 033246.

Shor, P. W., 1997, Polynomial-time algorithms for prime factorization and discrete logarithms on a quantum computer: SIAM Journal on Computing, **26**, 1484–1509.

Chapter 2

Seismic Traveltime Inversion with Quantum Computing

Hoang Anh Nguyen

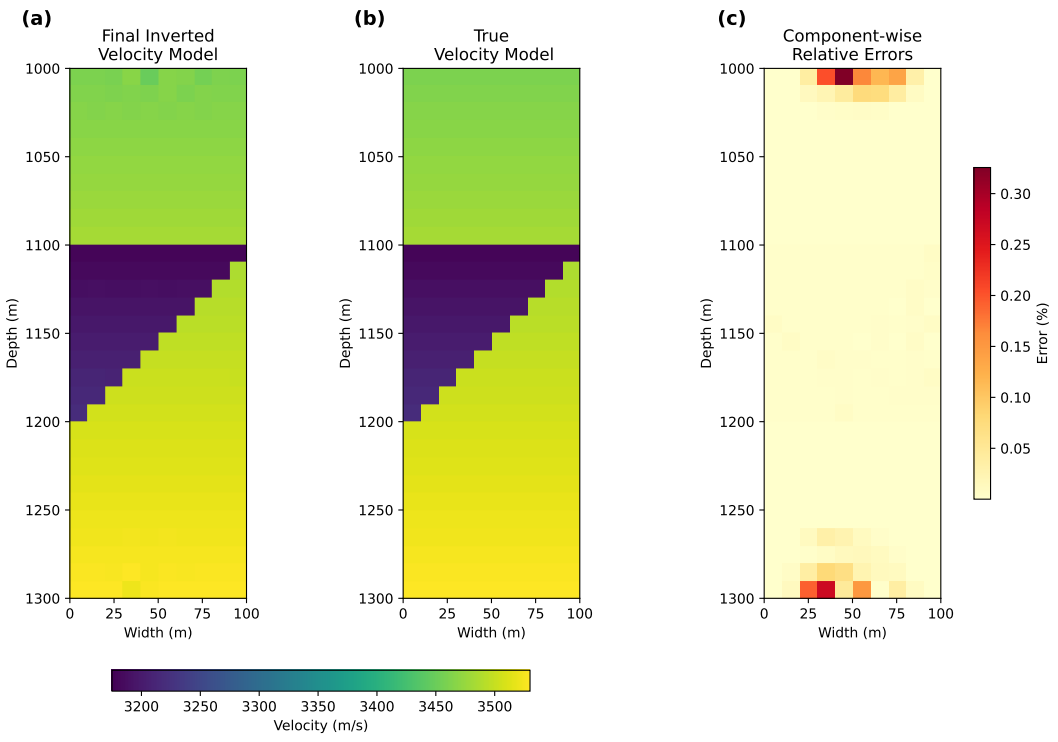

Summary

Project Goals

- Demonstrate the feasibility of applying quantum annealing to seismic traveltime inversion using a synthetic velocity model representing a carbon storage reservoir.
- Evaluate the performance of the D-Wave Advantage quantum annealer compared to classical least squares methods, particularly under noisy data conditions.
- Develop and test a recursive quantum inversion workflow, aiming to achieve accurate velocity reconstructions within a limited number of iterations.

Data

The synthetic travel-time data is generated from a velocity model representing a carbon storage reservoir. This data is then used as input for the inversion process.

Introduction

Quantum computing is an emerging field with significant promise for various scientific and engineering disciplines. As we stand at the frontier of this technological revolution, early-stage research in quantum computing is crucial for the advancement of geophysics. Numerous studies have begun to explore the integration of quantum computing within this field, highlighting its immense and revolutionary potential Moradi et al. (2018). For instance, quantum annealers can perform well in solving tomography optimization problems Sarkar and Levin (2018). The quantum computing is applied for binary-value full waveform inversion, addressing issues related to velocity variations Greer and O'Malley (2020). In the frequency domain, the seismic wave equation can be reduced to a system of linear equations, allowing for the application of quantum annealing of Petroleum Engineers (2022). Furthermore, it has been shown that quantum annealing impedance inversion with L1 norm regularization can dramatically enhance accuracy and anti-noise capabilities Wang et al. (2024).

A quantum annealer is a specific type of quantum computer designed to solve optimization problems Yulianti and Surendro (2022). The quantum annealing process in quantum annealers can find the minimum energy state of a system, corresponding to the optimal solution of a given problem McGeoch (2020). This process is achieved by utilizing quantum fluctuations, allowing the system to tunnel through energy barriers Crosson and Harrow (2016). While there are various types of models in quantum computing Nimbe et al. (2021); Lu et al. (2023), this particular feature allows quantum annealing to efficiently explore complex energy landscapes, making them particularly well-suited for solving optimization problems.

Most previous attempts to address seismic problems using quantum annealers have primarily involved relatively simple models Alu (2015); Albino et al. (2022). For conventional approach by classical computers, the cross-well seismic inversion between boreholes can be computationally expensive McMechan (1983), necessitating the development of new methods to tackle these challenges. Therefore, in this study, we aim to advance this line of research by applying quantum annealing to a complex problem: Seismic traveltime inversion of the velocity model between two boreholes. Our focus is on developing an inversion strategy that can accurately invert the velocity model with noisy data despite the limitation of the quantum hardware, specifically targeting carbon storage scenarios at depths of 1000-1300 meters. We use quantum annealer at D-Wave Advantage System, which has at least 5000 qubits McGeoch and Farré (2020). Clearly, this travel-time inversion method can be applied to other acquisition geometries and data such as surface seismic, vertical seismic profile (VSP), earthquake or micro seismic data.

Data Acquisition

We construct a velocity model representing carbon storage applications, as shown in Fig. 2.1a. This model spans a depth range from 1000 m to 1300 m and extends 100 m horizontally. The size of the grid cell for this model is 10 x 10 m. Within this model, the carbon storage structure is depicted as a wedge, starting from 1100 m and reaching a maximum depth of 1200 m. The velocity model is constructed with varying velocities to reflect real-world geological conditions.

The average velocity within the carbon storage area ranges from 3180 to 3220 m/s, which is about 11% lower than the surrounding background velocity, which ranges from 3530 to 3640 m/s. Furthermore, the velocities increase with depth.

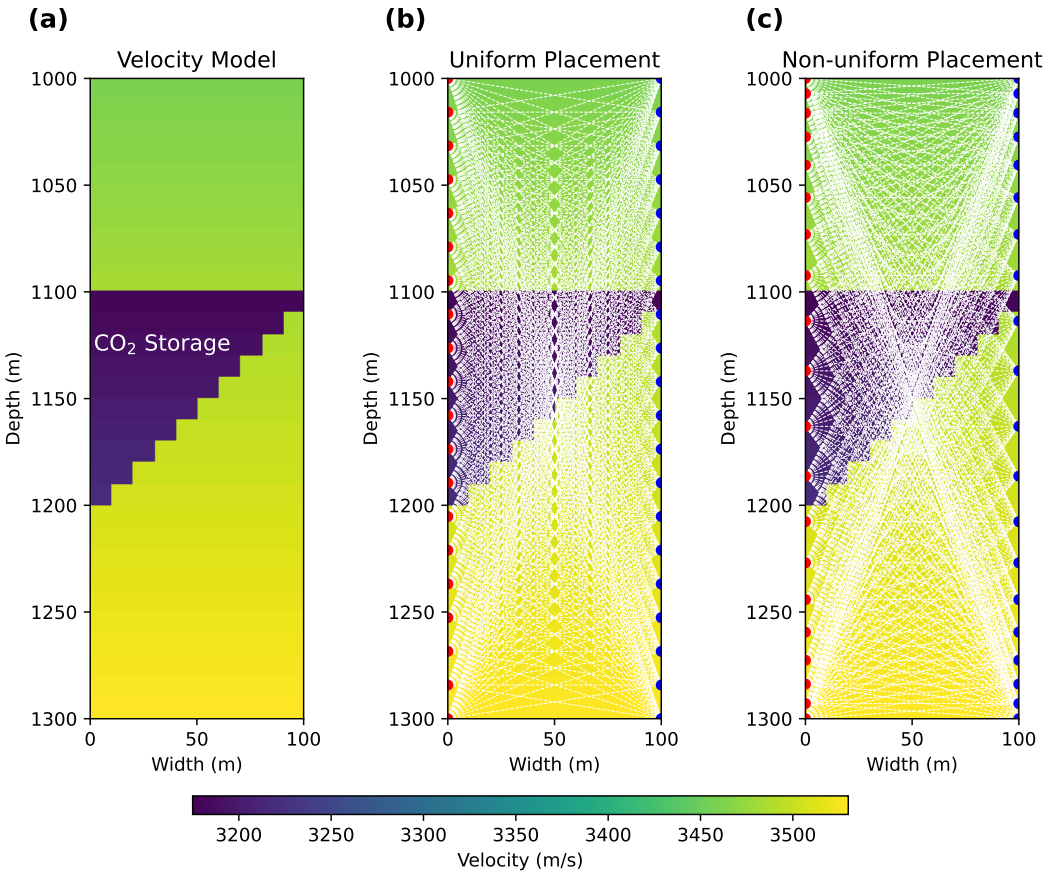

Figure 2.1: The carbon storage velocity model and ray coverage patterns. Red dots are sources, blue dots are receivers, and white lines represent the ray paths. (a) The synthetic velocity model with a wedge-shaped low-velocity carbon storage formation. (b) Ray coverage from sources and receivers placed in a uniform grid within two boreholes. (c) Ray coverage from sources and receivers placed in a non-uniform pattern, enhancing coverage and constraints for the quantum annealing process.

The uniform placement (Fig. 2.1b) is commonly used in seismic data acquisition for simplicity in boreholes. However, this approach results in significantly lower ray coverage in the shallow and deep sections compared to the middle section. To address these limitations, in our survey, 20 pairs of sources and receivers are non-uniformly deployed within two boreholes (Fig. 2.1c). The non-uniform deployment is designed to introduce more constraints for the quantum annealing process, thereby improving the overall accuracy of the seismic inversion. The sources and receivers of non-uniform placement are distributed according to a quadratic polynomial distribution.

Annealing Methods

Quantum computing is rapidly emerging as a pivotal area of scientific and technological advancement, attracting considerable investment and interest due to its profound potential Britt and Humble (2017); Möller and Vuik (2017); Coccia et al. (2024). Unlike classical computers that use bits, which exist only in states of 0 or 1, quantum computers employ quantum bits, or qubits. Qubits possess unique properties such as superposition, entanglement, and interference Qiao et al. (2018); Neeley et al. (2010); Loft et al. (2020), enabling them to perform certain complex computations beyond the capabilities of classical computers Feld et al. (2019); Neukart et al. (2017). Qubits can be constructed from various physical systems such as photons, trapped atoms, nuclear magnetic resonance, quantum dots, dopants in solids, and superconductors Ladd et al. (2010). Previous research Baldassi and Zecchina (2018); Denchev et al. (2016); Albash and Lidar (2018); Nakata and Murao (2014); Senekane (2021) has provided evidence that quantum computing possibly surpasses classical computers in terms of processing speed and efficiency for certain problems.

The quantum annealing process facilitates the finding of the global minimum of a cost function efficiently. This process can be described using the real-time Schrödinger equation Morita and Nishimori (2008):

$$i\hbar\frac{d}{dt}|\Psi(t)\rangle = H(t)|\Psi(t)\rangle \tag{2.1}$$

where $|\cdot\rangle$ is the ket of the Dirac notation Dirac (1939), i is the imaginary unit, t is time, $\hbar$ is the reduced Planck's constant, $\Psi(t)$ is the wave function, $|\Psi(t)\rangle$ is the quantum state vector, H is the Hamiltonian representing the total energy of the quantum system Griffiths and Schroeter (2018); Shankar (1994). If $\hbar$ is set as 1, the Eq. 2.1 becomes:

$$i\frac{d}{dt}|\Psi(t)\rangle = H(t)|\Psi(t)\rangle \tag{2.2}$$

The Hamiltonian in quantum annealing can be composed of two components Rajak et al. (2023); Biswas et al. (2017):

$$H(t) = A(t)H_0 + B(t)H_1 \tag{2.3}$$

where H_0 is the initial Hamiltonian, representing a system with an initial ground state. H_1 is the final Hamiltonian, whose ground state encodes the solution to the optimization problem. $A(t)$ and $B(t)$ are time-dependent coefficients. $A(t)$ and $B(t)$ are set in a range of 0 to 1 so that $A(t_0) \gg B(t_0)$ at the initial time t_0 and $B(t_1) \gg A(t_1)$ at the final time t_0. During the process, $A(t)$ monotonically decreases, while $B(t)$ monotonically increases. At the start of the annealing process, $H(t) \approx H_0$. At the end of the annealing process, $H(t) \approx H_1$. Thus, the system transitions from the ground state of H_0 to the ground state of H_1. If $H(t)$ changes sufficiently slowly, the state evolves adiabatically Hauke et al. (2020).

The problems are then often mapped onto a Quadratic Unconstrained Binary Optimization (QUBO) or Ising model Willsch et al. (2022):

$$\text{QUBO:} \quad \min_{x_j=0,1}\left(\sum_{j\leq k} x_j Q_{jk} x_k + C_1\right) \tag{2.4}$$

$$\text{Ising:} \quad \min_{s_j=\pm 1} \left(\sum_j h_j s_j + \sum_{j<k} J_{jk} s_j s_k + C_2 \right) \tag{2.5}$$

where j, k are indices, ranging over all qubits. In the QUBO model (Eq. 2.4), Q_{jk} is the QUBO matrix with values $Q_{jk} \in \mathbb{R}$. The binary variable vector is $\mathbf{x}$ with $x_j \in \{0, 1\}$. In the Ising model (Eq. 2.5), the problem is defined by the biases $h_j \in \mathbb{R}$ and the couplers $J_{jk} \in \mathbb{R}$, and the binary variable vector is $\mathbf{s}$ with $s_j \in \{-1, 1\}$. C_1 and C_2 are constants which do not affect the solution of the optimization problem. The Ising model and the QUBO model are mathematically equivalent, allowing them to be translated into each other. This equivalence provides a flexible approach to problem-solving, enabling the conversion of problems between these models based on the requirements and available tools. There are also tools, such as `ToQUBO.jl`, designed to convert standard problems into the QUBO format Xavier et al. (2023). In this paper, we utilize the quantum annealer from D-Wave Advantage Systems McGeoch and Farré (2020) to employ direct quantum processing unit (QPU) methods for seismic travel inversion.

Transforming Ray Equations to QUBO

The inversion problem need to be translated to the QUBO formula. The set of ray equations can be represented as McMechan (1983):

$$\mathbf{Ds} = \mathbf{T}, \tag{2.6}$$

where $\mathbf{D}$ is the matrix of distance increments d_j, $\mathbf{s}$ is the slowness vector, and $\mathbf{T}$ is the travel time vector. The size of $\mathbf{D}$ can be very large, therefore solving for $\mathbf{s}$ through matrix operations on $\mathbf{D}$ is computationally intensive. This challenge is exacerbated by the relatively sparse and random distribution of elements within $\mathbf{D}$. Consequently, alternative methods are required to solve these problems efficiently while maintaining accuracy. Quantum annealers can provide quantum metaheuristic algorithms to address this issue. Eq. 2.6 can be solved by minimizing the objective function:

$$f(\mathbf{s}) = \|\mathbf{Ds} - \mathbf{T}\|_2^2 . \tag{2.7}$$

The objective function $f(\mathbf{s})$ computes the difference between the observed travel times and those predicted by the model given a slowness vector $\mathbf{s}$. Minimizing this function ensures that the model's predictions align as closely as possible with the observed data, thus achieving an optimal fit. Quantum annealers offer a direct approach to solving binary objective functions O'Malley and Vesselinov (2016):

$$f(\mathbf{q}) = \left\|\mathbf{A}^d\mathbf{q} - \mathbf{b}\right\|_2^2 . \tag{2.8}$$

In this formulation, $\mathbf{q}$ is a binary vector, $\mathbf{A}^d$ is a real-valued matrix, and $\mathbf{b}$ is a real-valued vector. Because quantum computers are designed to solve QUBO problems, transforming real-valued variables to binary values is essential. However, the number of binary variables n_{binary} increases with the number of bits R used for fixed-point approximation, and it is related to the number of real-valued variables n_{real} as $n_{\text{binary}} = n_{\text{real}} \times R$. Higher values of R yield greater accuracy in representing the floating-point numbers, but the current limitations

of quantum computer hardware restrict the number of qubits available. To address this issue without excessively increasing the number of binary variables, the initial velocity guess, variable boundaries Souza et al. (2022) and recursive methods Rogers and Singleton (2020) are employed. The initial guess and the boundaries are used to rescale the range of the slowness vector $\mathbf{s}$ to a new vector $\mathbf{x}$ such that $x_i \in [0, 2)$, facilitating easier binary representation. Recursive methods are then applied to enhance the precision of floating-point divisions. These methods iteratively refine the estimate of $\mathbf{s}$, reducing the error at each step. The initial objective function Eq. 2.7 can be reformulated as:

$$f(\mathbf{x}) = \|\mathbf{D}\mathbf{x} - \mathbf{b}\|_2^2, \tag{2.9}$$

where $\mathbf{b} = (\mathbf{T} + L\mathbf{I} - \mathbf{D}\mathbf{s}_0)/L$, L is the variable boundaries, $\mathbf{s}_0$ is the initial guess of the slowness vector, and $\mathbf{I}$ is the identity vector. The slowness vector $\mathbf{s}$ is then in the range of $[\mathbf{s}_0 - L\mathbf{I}; \mathbf{s}_0 + L\mathbf{I}]$. This range ensures that the solution space is adequately covered. To express this as a binary objective function, x_i is represented in binary form using the R bit fixed-point approximation:

$$x_i = \sum_{r=0}^{R-1} 2^{-r} q_r, \tag{2.10}$$

where $q_r \in \{0, 1\}$ is the value of the r-th bit. This transformation is essential for harnessing the computational power of quantum annealers, which are inherently designed to solve binary optimization problems. The new matrix $\mathbf{A}^d$ in Eq. 2.8 is derived from $\mathbf{D}$ and R such that $\mathbf{D}\mathbf{x} = \mathbf{A}^d\mathbf{q}$. The QUBO matrix Q_{ij} in Eq. 2.4 is then constructed from the given matrix $\mathbf{D}$ and the calculated vector $\mathbf{b}$ O'Malley and Vesselinov (2016); Borle and Lomonaco (2019):

$$Q_{jj} = \sum_i A_{ij}(A_{ij} - 2b_j), \tag{2.11}$$

$$Q_{jk} = 2\sum_i A_{ij}A_{ik}. \tag{2.12}$$

The QUBO matrix is directly input into the Quantum Processing Unit (QPU). The system utilizes `DWaveSampler()` to employ a D-Wave system as the sampler. Subsequently, `EmbeddingComposite()` manages the mapping between the problem and the D-Wave system's numerically indexed qubits, a process known as minor-embedding D-Wave Systems Inc (2023).

In this study, we perform traveltime inversion using $R = 3$ for 10 iterations with quantum annealing. The total number of real-valued variables of the problem is 300. Due to quantum hardware limitations, we break down the model into 30 layers with 10 variables each. This division reduces the complexity of each sub-problem, making it manageable for the quantum processor and allowing for better control of the boundary L. Since the problem from Eq. 2.6 is depth-independent, we simplify the process by adjusting the system's coordinates at each iteration. The approach ensures that each layer is treated independently, reducing the overall complexity of the inversion. By implementing these techniques, we can efficiently solve large-scale traveltime inversion problems using quantum annealers.

Results

We start the quantum annealing inversion process with exact traveltime data without noise and constant initial velocity model v_{ini} of 3475 m/s. The initial model and the results of the inverted model v_{inv} at each iteration obtained after the first 9 iterations indicate rapid convergence (Fig. 2.2). Notably, in the first iteration, the carbon storage area is immediately identified with high precision.

The component-wise relative errors e_{ij} between the true $v_{true,ij}$ and final inverted velocity model $v_{final,ij}$ after 10 iterations is shown in Fig. 2.3. The component-wise relative errors are calculated by $e_{ij} = |v_{inv,ij} - v_{true,ij}|/|v_{true,ij}|$. The most significant errors occurs in the shallow and deep regions with weakest constraints, yielding a maximum relative error value of about 0.326%. In contrast, the carbon storage area, spanning depths from 1100 to 1200 m, demonstrates exceptionally low errors due to the high ray coverage. The high-accuracy result underscores the effectiveness of the quantum annealing approach to the traveltime inversion.

For seismic traveltime inversion problem, the quantum annealing method and the classical linear least squares approach produce similar levels of error under ideal conditions, where data is free of noise Souza et al. (2022). However, real-world data often contain random noise, making it essential to assess the robustness of these methods under realistic conditions. Since we use the first-arrival traveltime, the data is relatively clean Daley et al. (2008). Therefore, we introduce the random noise in a range from 1% to 5% into the synthetic data. We compare the outcomes of the Tikhonov regularization least squares, serving as the standard method, with that of the quantum annealing method.

The results reveal a stark contrast in the sensitivity of these methods to noise. In this problem, the Tikhonov regularization linear least squares method is sensitive to noise (Fig. 2.4a, b, c). At the noise level of 1% of the traveltime, while this method can identify the region of carbon storage, the deviation of the inverted model from true model is considerable. As the noise level increases to 2% and 5% of the traveltime, the linear least squares method almost fails to accurately determine the velocity model. This significant sensitivity limits its effectiveness in processing noisy seismic data, posing challenges for practical applications. In contrast, with the same noise, the quantum annealing method is more robust (Fig. 2.4d, e, f). At the 1% noise level, the differences between the noise-free model and the results obtained are small. Differences start to appear primarily in shallow and deep areas where there is less constraint. Remarkably, at the 5% noise level, the quantum annealing method still effectively reproduces the velocity model. In areas with high ray coverage, these differences are small. This analysis underscores the potential of quantum annealing method for handling noisy seismic data more effectively than the classical linear least squares method.

Tikhonov Regularization Linear Least Squares Inversion

For ill-conditioned problems, small changes in $\mathbf{D}$ or $\mathbf{T}$ can lead to significant variations in the results Deif (1986). To mitigate the effects of noise in the data, we employ Tikhonov regularization methods. The new objective function (Eq. 2.7) can be expressed as a general

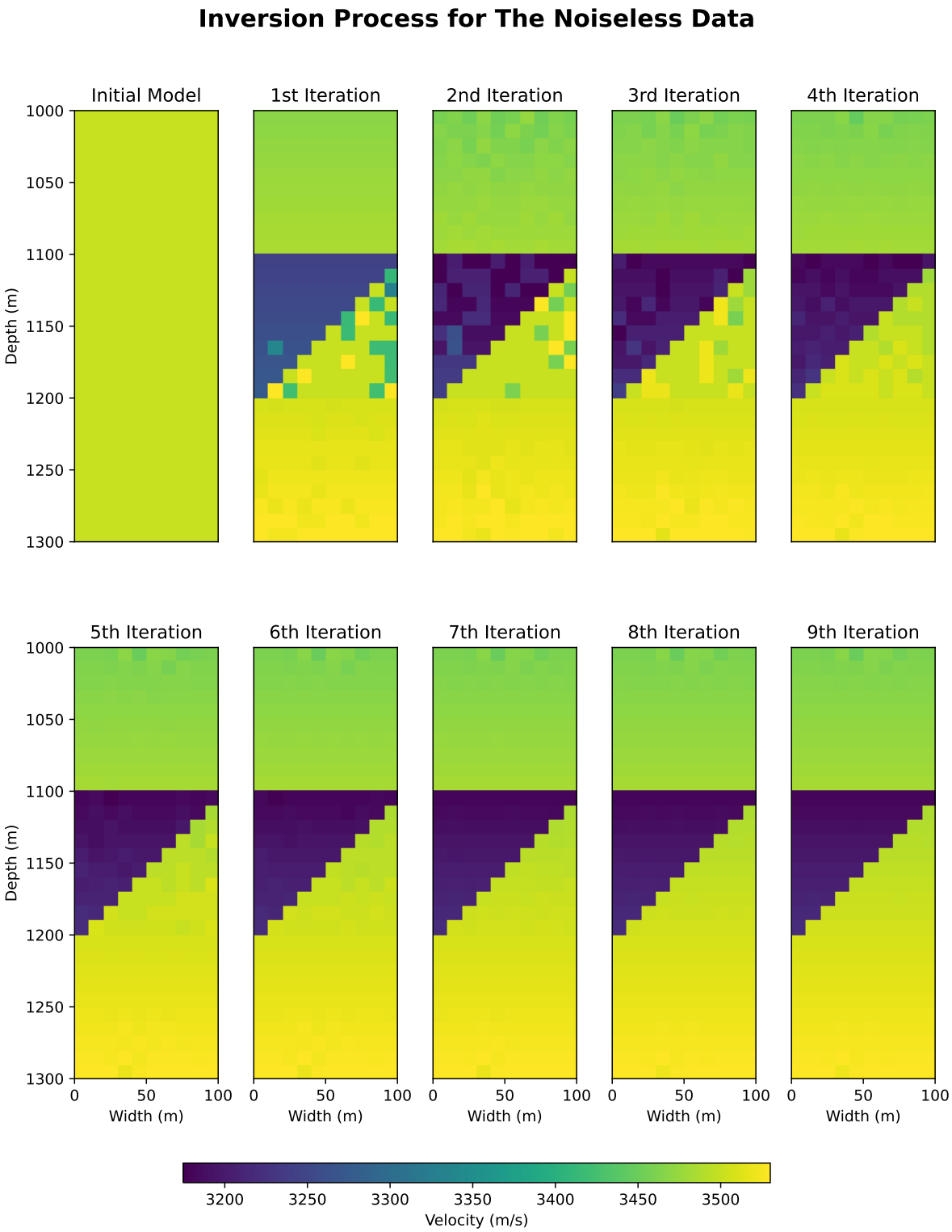

Figure 2.2: The starting model v_{ini} and the inverted velocity model v_{inv} over the first 9 iterations with exact, noise-free traveltime data.

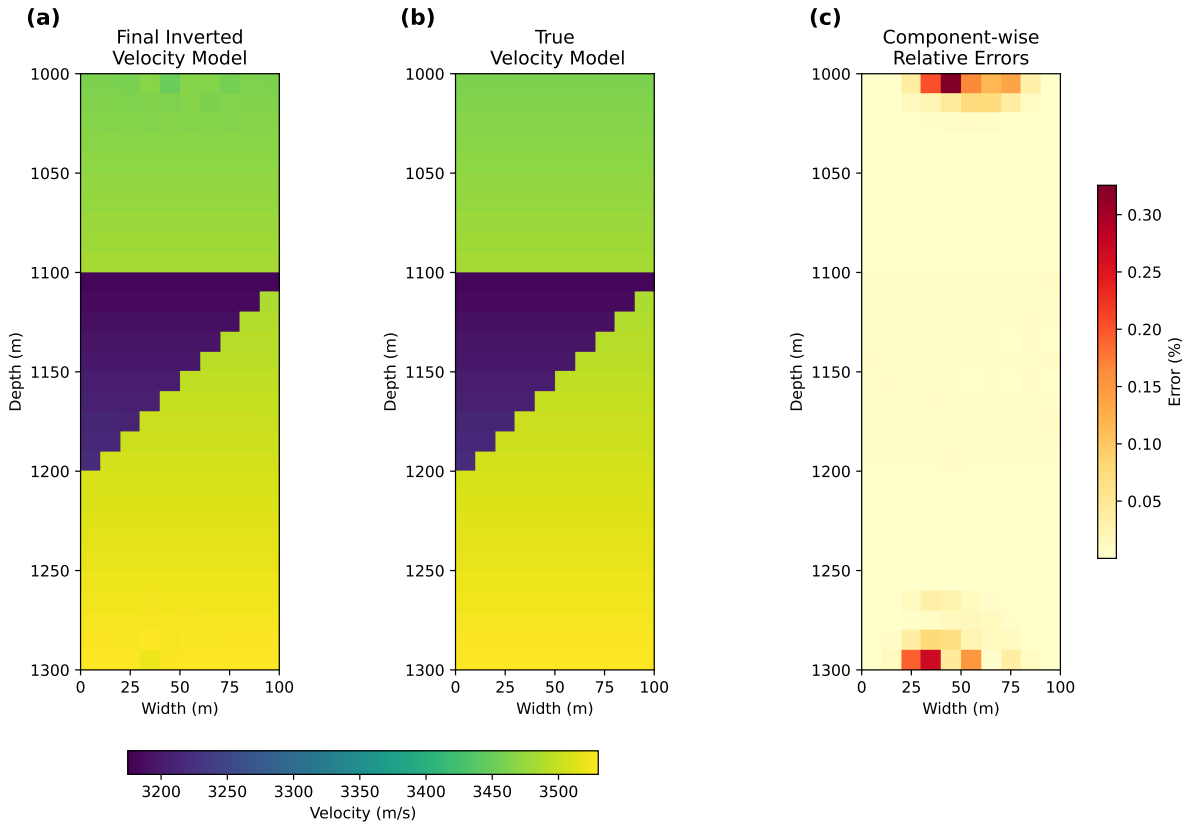

Figure 2.3: Velocity models and error: (a) final noiseless inverted model after 10 iterations $v_{inv,ij}$, (b) true model $v_{true,ij}$, and (c) the component-wise relative errors e_{ij} between the final inverted and true velocity model.

regularized form Fierro et al. (1997):

$$f_\lambda(\mathbf{s}) = \|\mathbf{D}\mathbf{s} - \mathbf{T}\|_2^2 + \lambda g(\mathbf{s}), \tag{2.13}$$

where λ is the regularization parameter controlling the trade-off between the data fidelity term $\|\mathbf{D}\mathbf{s} - \mathbf{T}\|_2^2$ and the regularization term $g(\mathbf{s})$. The Tikhonov regularization is flexible and allows different types of regularization functions. The standard Tikhonov regularization with L_2-norm is in the form:

$$f_\lambda(\mathbf{s}) = \|\mathbf{D}\mathbf{s} - \mathbf{T}\|_2^2 + \lambda\|\mathbf{s}\|_2^2 \tag{2.14}$$

where $\|\mathbf{s}\|_2^2 = \mathbf{s}^T\mathbf{s}$ penalizes large values in the solution. Another form is the first-order Tikhonov regularization with a smoothness regularization:

$$f_\lambda(\mathbf{s}) = \|\mathbf{D}\mathbf{s} - \mathbf{T}\|_2^2 + \lambda\|D_1\mathbf{s}\|_2^2 \tag{2.15}$$

where D_1 is the first-order difference operator which enforces smooth variation in $\mathbf{s}$ by penalizing large first derivatives. Similarly, second-order Tikhonov regularization penalizes the curvature of the solution:

$$f_\lambda(\mathbf{s}) = \|\mathbf{D}\mathbf{s} - \mathbf{T}\|_2^2 + \lambda\|D_2\mathbf{s}\|_2^2 \tag{2.16}$$

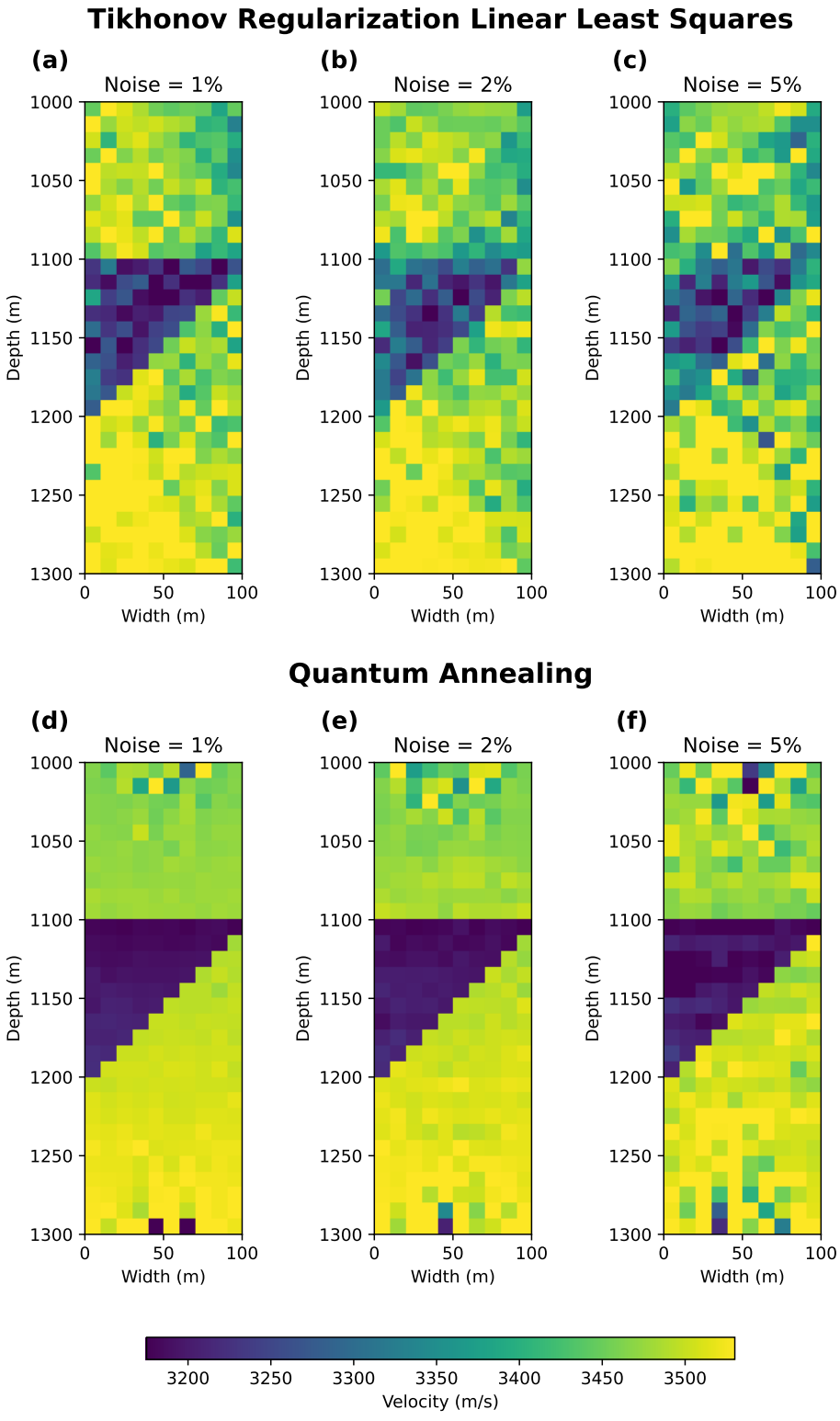

Figure 2.4: Traveltime inversion results with different noisy data using linear least squares (a, b, c) and quantum annealing method (d, e, f)

where D_2 is the second-order difference operator which enforces smooth curvature by penalizing large second derivatives. In general, $g(\mathbf{s})$ can be $g(\mathbf{s}) = \|\mathbf{s}\|_2^2$ for standard L_2-norm regularization, $g(\mathbf{s}) = \|D_1\mathbf{s}\|_2^2$ for first-order smoothness, or $g(\mathbf{s}) = \|D_2\mathbf{s}\|_2^2$ for second-order smoothness. The choice of $g(\mathbf{s})$ depends on prior knowledge and the desired properties of the solution. Here, we use a custom Tikhonov regularization $g(\mathbf{s}) = \|\mathbf{s} - \mathbf{s}_0\|_2^2$, where $\mathbf{s}_0$ is the initial guess for the slowness and is chosen as the input for the quantum annealing process. The objective function is now expressed as:

$$f_\lambda(\mathbf{s}) = \|\mathbf{D}\mathbf{s} - \mathbf{T}\|_2^2 + \lambda\|\mathbf{s} - \mathbf{s}_0\|_2^2. \tag{2.17}$$

The solution to this regularized problem is given by:

$$\mathbf{s} = \left(\mathbf{D}^T\mathbf{D} + \lambda\mathbf{I}\right)^{-1}\left(\mathbf{D}^T\mathbf{T} + \lambda\mathbf{s}_0\right). \tag{2.18}$$

Cost Analysis

Quantum annealing directly solves $f(\mathbf{q}) = \left\|\mathbf{A}^d\mathbf{q} - \mathbf{b}\right\|_2^2$ (Eq. 2.8) by providing the solution binary vector $\mathbf{q}$. The quantum annealing process involves three sources of computational cost: preparing the binary problem, executing the annealing on the quantum hardware, and post-processing the results. The cost of preparing and post-processing is $\mathcal{O}(mn^2 + mnc + n^2c^2)$. For a single iteration of the loop, the cost of executing the annealing process on the quantum hardware is $\mathcal{O}(\mathcal{P}(cn))$. Here, m and n represent the rows and columns of the matrix $\mathbf{D}$, respectively. $\mathcal{P}(cn)$ is a polynomial term. The parameter $c = |\Theta| + 1$, where Θ used for representing the variables x_j as a fixed-point approximation in terms of power of 2 (Eq. 2.10). The general form of the set Θ is defined as Borle and Lomonaco (2019):

$$\Theta = \{2^l : l \in [o, p] \wedge l, o, p \in \mathbb{Z}\}, \tag{2.19}$$

where l is contiguous integer values within the interval $[o, p]$, and o and p are the lower and upper bounds of the interval. In our scheme, instead of using a large range for o and p, we refine the precision of x_i iteratively over multiple loops to achieve higher accuracy. For a 3-bit fixed-point approximation with $x_i \in [0, 2)$, $o = 0$ and $p = -2$. For the K iterations, the total cost for process is:

$$\mathcal{O}(mn^2 + mnc + n^2c^2 + K \cdot \mathcal{P}(cn)), \tag{2.20}$$

For Tikhonov regularization methods with the direct solver (e.g., LU decomposition), the computational cost primarily depends on solving the modified linear system. The cost for finding $\mathbf{s}$ with a given λ is $\mathcal{O}(mn^2 + n^3)$. Selecting the optimal λ is crucial for achieving a balance between data fidelity and regularization. One commonly used technique is the L-curve method, which plots the norm of the regularization term $\|R(\mathbf{s})\|$ against the residual norm $\|\mathbf{D}\mathbf{s} - \mathbf{T}\|$ on a log-log scale Hansen (2000); Calvetti et al. (2000). For N_λ values of λ, the cost of solving the Tikhonov-regularized system for each λ is $\mathcal{O}(N_\lambda \cdot (mn^2 + n^3))$. In addition, the computation of the residual norm $\|\mathbf{D}\mathbf{s} - \mathbf{T}\|$ for each λ involves matrix-vector multiplications, contributing a cost of $\mathcal{O}(N_\lambda \cdot mn)$. If we want to find the optimal λ automatically, the curvature of the L-curve must be computed. This requires additional operations such as numerical

differentiation and curvature estimation, which are negligible compared to the cost of solving the regularized systems. Thus, the total cost for the L-curve method, including the automatic selection of λ, is:

$$\mathcal{O}(N_\lambda \cdot (mn^2 + n^3)). \tag{2.21}$$

From Eqs. 2.20 and 2.21, achieving a computational cost of $\mathcal{O}(\mathcal{P}(cn)) < \mathcal{O}(n^3)$ would enable quantum annealing to significantly accelerate problem-solving. Research efforts, such as those utilizing multi-qubit correction techniques Dorband (2018), aim to realize this improvement. These approaches can potentially achieve a substantial reduction in computational complexity. This advancement would facilitate rapid convergence to the global minimum and unlock considerable performance gains.

Discussion

In this study, we demonstrate several advancements to enhance the robustness and accuracy of seismic traveltime inversion results using the quantum annealing method. A significant improvement involves incorporating non-uniform source and receiver spacing. By using non-uniform spacing, we achieve better ray coverage of both shallow and deep regions, thereby increasing the overall accuracy of the final inverted velocity model.

The initial problem is broken down into smaller sub-problems, we also introduce the boundary L during the inversion process for better constraint and accommodating hardware limitations. While this paper does not utilize parallel processing, solving these sub-problems independently enables parallel execution, which can significantly reduce computational time.

For practical applications where noise is an unavoidable factor, our method demonstrates a remarkable ability to handle noisy data effectively and is highly suitable for the ill-conditioned problems, maintaining high efficiency and accuracy. The key advantage of the quantum annealing method is its ability to locate the global minimum of the objective function more effectively than classical methods, which are often trapped in local minima. Quantum tunneling allows the quantum system to explore a broader solution space and tunnel barriers that would hinder classical optimization methods Finnila et al. (1994). This method can result in more accurate and reliable inversion outcomes, particularly in complex and heterogeneous environments. The quantum annealer solves problems using principles of quantum mechanics, which inherently depend on the operating environment of the machine. Consequently, running the same problem multiple times may yield slightly different results because of the probabilistic nature of quantum computations Pérez-Delgado and Kok (2011); Hevia et al. (2021). However, we expect the advancements in quantum technology will decrease this variability and also reduce computational time.

Conclusion

The integration of quantum annealing in seismic traveltime inversion represents a potentially major advancement in geophysics. We utilise the open-access D-Wave Advantage quantum

annealer to solve the inversion problem for a synthetic velocity model, representing a carbon storage scenario. The quantum annealing recursive method can give a good inverted velocity result after 10 iterations. Notably, the quantum method outperforms the classical linear least squares method in dealing with noisy data, where classical methods sometimes struggle. Despite promising results, the current state of quantum computing is not without its challenges. The slight variability in the results due to quantum noise Li et al. (2020); França and García-Patrón (2021); de Leon et al. (2021) requires multiple runs to ensure reliable results. However, these challenges are expected to diminish as advances in quantum technology continue. This study suggests that quantum annealing could revolutionize seismic inversion processes, offering more accurate solutions in scenarios where traditional methods are computationally intensive or even infeasible. As quantum computing matures, its applications in geophysics are likely to expand, encompassing more complex and larger-scale problems. This research not only underscores the potential of quantum annealing in seismic inversion but also sets the stage for future exploration into other areas of inverse problems. We expect that continued development of quantum computing technologies promises to unlock new capabilities, possibly making it an indispensable tool for new challenges.

Bibliography

2015, Prestack Seismic Inversion by Quantum Annealing: Application To Cana Field: volume **All Days** *of* SEG International Exposition and Annual Meeting.

Albash, T., and D. A. Lidar, 2018, Demonstration of a scaling advantage for a quantum annealer over simulated annealing: Phys. Rev. X, **8**, no. 3, 031016.

Albino, A. S., O. M. Pires, P. Nogueira, R. F. de Souza, and E. G. S. Nascimento, 2022, Quantum computational intelligence for traveltime seismic inversion.

Baldassi, C., and R. Zecchina, 2018, Efficiency of quantum vs. classical annealing in nonconvex learning problems: Proceedings of the National Academy of Sciences, **115**, 1457–1462.

Biswas, R., Z. Jiang, K. Kechezhi, S. Knysh, S. Mandrà, B. O'Gorman, A. Perdomo-Ortiz, A. Petukhov, J. Realpe-Gómez, E. Rieffel, D. Venturelli, F. Vasko, and Z. Wang, 2017, A nasa perspective on quantum computing: Opportunities and challenges: Parallel Computing, **64**, 81–98. (High-End Computing for Next-Generation Scientific Discovery).

Borle, A., and S. J. Lomonaco, 2019, Analyzing the quantum annealing approach for solving linear least squares problems: WALCOM: Algorithms and Computation, Springer International Publishing, 289–301.

Britt, K. A., and T. S. Humble, 2017, High-performance computing with quantum processing units: J. Emerg. Technol. Comput. Syst., **13**.

Calvetti, D., S. Morigi, L. Reichel, and F. Sgallari, 2000, Tikhonov regularization and the l-curve for large discrete ill-posed problems: Journal of Computational and Applied Mathematics, **123**, 423–446. (Numerical Analysis 2000. Vol. III: Linear Algebra).

Coccia, M., S. Roshani, and M. Mosleh, 2024, Evolution of quantum computing: Theoretical and innovation management implications for emerging quantum industry: IEEE Transactions on Engineering Management, **71**, 2270–2280.

Crosson, E., and A. W. Harrow, 2016, Simulated quantum annealing can be exponentially faster than classical simulated annealing: 2016 IEEE 57th Annual Symposium on Foundations of Computer Science (FOCS), 714–723.

D-Wave Systems Inc, 2023, dwave-system documentation. (Release 1.18.0).

Daley, T. M., L. R. Myer, J. E. Peterson, E. L. Majer, and G. M. Hoversten, 2008, Time-lapse crosswell seismic and vsp monitoring of injected co2 in a brine aquifer: Environmental Geology, **54**, 1657–1665.

de Leon, N. P., K. M. Itoh, D. Kim, K. K. Mehta, T. E. Northup, H. Paik, B. S. Palmer, N. Samarth, S. Sangtawesin, and D. W. Steuerman, 2021, Materials challenges and opportunities for quantum computing hardware: Science, **372**, eabb2823.

Deif, A., 1986, *in* Perturbation of Linear Equations: Springer Berlin Heidelberg, 1–43.

Denchev, V. S., S. Boixo, S. V. Isakov, N. Ding, R. Babbush, V. Smelyanskiy, J. Martinis, and H. Neven, 2016, What is the computational value of finite-range tunneling?: Phys. Rev. X, **6**, no. 3, 031015.

Dirac, P. A. M., 1939, A new notation for quantum mechanics: Mathematical Proceedings of the Cambridge Philosophical Society, **35**, 416–418.

Dorband, J. E., 2018, A method of finding a lower energy solution to a qubo/ising objective function.

Feld, S., C. Roch, T. Gabor, C. Seidel, F. Neukart, I. Galter, W. Mauerer, and C. Linnhoff-Popien, 2019, A hybrid solution method for the capacitated vehicle routing problem using a quantum

annealer: Frontiers in ICT, **6**.
Fierro, R. D., G. H. Golub, P. C. Hansen, and D. P. O'Leary, 1997, Regularization by truncated total least squares: SIAM Journal on Scientific Computing, **18**, 1223–1241.
Finnila, A., M. Gomez, C. Sebenik, C. Stenson, and J. Doll, 1994, Quantum annealing: A new method for minimizing multidimensional functions: Chemical Physics Letters, **219**, 343–348.
França, D. S., and R. García-Patrón, 2021, Limitations of optimization algorithms on noisy quantum devices: Nature Physics, **17**, 1221–1227.
Greer, S., and D. O'Malley, 2020, *in* An approach to seismic inversion with quantum annealing: Society of Exploration Geophysicists, 2845–2849.
Griffiths, D. J., and D. F. Schroeter, 2018, Introduction to quantum mechanics, 3 ed.: Cambridge University Press.
Hansen, P., 2000, The l-curve and its use in the numerical treatment of inverse problems: Presented at the InviteComputational Inverse Problems in Electrocardiology, WIT Press. (InviteComputational Inverse Problems in Electrocardiology ; Conference date: 01-01-2000).
Hauke, P., H. G. Katzgraber, W. Lechner, H. Nishimori, and W. D. Oliver, 2020, Perspectives of quantum annealing: methods and implementations: Reports on Progress in Physics, **83**, 054401.
Hevia, J. L., G. Peterssen, C. Ebert, and M. Piattini, 2021, Quantum computing: IEEE Software, **38**, 7–15.
Ladd, T. D., F. Jelezko, R. Laflamme, Y. Nakamura, C. Monroe, and J. L. O'Brien, 2010, Quantum computers: Nature, **464**, 45–53.
Li, R. Y., T. Albash, and D. A. Lidar, 2020, Limitations of error corrected quantum annealing in improving the performance of boltzmann machines: Quantum Science and Technology, **5**, 045010.
Loft, N. J. S., M. Kjaergaard, L. B. Kristensen, C. K. Andersen, T. W. Larsen, S. Gustavsson, W. D. Oliver, and N. T. Zinner, 2020, Quantum interference device for controlled two-qubit operations: npj Quantum Information, **6**, 47.
Lu, B., L. Liu, J.-Y. Song, K. Wen, and C. Wang, 2023, Recent progress on coherent computation based on quantum squeezing: AAPPS Bulletin, **33**, 7.
McGeoch, C., 2020, Theory versus practice in annealing-based quantum computing: Theoretical Computer Science, **816**, 169–183.
McGeoch, C., and P. Farré, 2020, The d-wave advantage system: An overview: D-Wave Systems Inc., Burnaby, BC, Canada, Tech. Rep.
McMechan, G. A., 1983, Seismic tomography in boreholes: Geophysical Journal International, **74**, 601–612.
Moradi, S., D. Trad, and K. A. Innanen, 2018, *in* Quantum computing in geophysics: Algorithms, computational costs, and future applications: Society of Exploration Geophysicists, 4649–4653.
Morita, S., and H. Nishimori, 2008, Mathematical foundation of quantum annealing: Journal of Mathematical Physics, **49**, 125210.
Möller, M., and C. Vuik, 2017, On the impact of quantum computing technology on future developments in high-performance scientific computing: Ethics and Information Technology, **19**, 253–269.
Nakata, Y., and M. Murao, 2014, Diagonal quantum circuits: Their computational power and applications: The European Physical Journal Plus, **129**, 152.

Neeley, M., R. C. Bialczak, M. Lenander, E. Lucero, M. Mariantoni, A. D. O'Connell, D. Sank, H. Wang, M. Weides, J. Wenner, Y. Yin, T. Yamamoto, A. N. Cleland, and J. M. Martinis, 2010, Generation of three-qubit entangled states using superconducting phase qubits: Nature, **467**, 570–573.

Neukart, F., G. Compostella, C. Seidel, D. von Dollen, S. Yarkoni, and B. Parney, 2017, Traffic flow optimization using a quantum annealer: Frontiers in ICT, **4**.

Nimbe, P., B. A. Weyori, and A. F. Adekoya, 2021, Models in quantum computing: a systematic review: Quantum Information Processing, **20**, 80.

of Petroleum Engineers, S., ed., 2022, Quantum Computation for End-to-End Seismic Data Processing with Its Computational Advantages and Economic Sustainability: volume **Day 2 Tue, November 01, 2022** *of* Abu Dhabi International Petroleum Exhibition and Conference.

O'Malley, D., and V. V. Vesselinov, 2016, Toq.jl: A high-level programming language for d-wave machines based on julia: 2016 IEEE High Performance Extreme Computing Conference (HPEC), 1–7.

Pérez-Delgado, C. A., and P. Kok, 2011, Quantum computers: Definition and implementations: Phys. Rev. A, **83**, no. 1, 012303.

Qiao, L.-F., A. Streltsov, J. Gao, S. Rana, R.-J. Ren, Z.-Q. Jiao, C.-Q. Hu, X.-Y. Xu, C.-Y. Wang, H. Tang, A.-L. Yang, Z.-H. Ma, M. Lewenstein, and X.-M. Jin, 2018, Entanglement activation from quantum coherence and superposition: Phys. Rev. A, **98**, no. 5, 052351.

Rajak, A., S. Suzuki, A. Dutta, and B. K. Chakrabarti, 2023, Quantum annealing: an overview: Philosophical Transactions of the Royal Society A: Mathematical, Physical and Engineering Sciences, **381**, 20210417.

Rogers, M. L., and R. L. Singleton, 2020, Floating-point calculations on a quantum annealer: Division and matrix inversion: Frontiers in Physics, **8**.

Sarkar, R., and S. A. Levin, 2018, *in* Snell tomography for net-to-gross estimation using quantum annealing: Society of Exploration Geophysicists, 5078–5082.

Senekane, M., 2021, Hands-on quantum information processing with python : get up and running with information processing and computing based on quantum mechanics using python: Packt. (englisch).

Shankar, R., 1994, *in* The Postulates—a General Discussion: Springer US, 115–150.

Souza, A. M., E. O. Martins, I. Roditi, N. Sá, R. S. Sarthour, and I. S. Oliveira, 2022, An application of quantum annealing computing to seismic inversion: Frontiers in Physics, **9**.

Wang, S., C. Liu, P. Li, C. Chen, and C. Song, 2024, Stable and efficient seismic impedance inversion using quantum annealing with L1 norm regularization: Journal of Geophysics and Engineering, **21**, 330–343.

Willsch, D., M. Willsch, C. D. G. Calaza, F. Jin, H. D. Raedt, M. Svensson, and K. Michielsen, 2022, Benchmarking advantage and d-wave 2000q quantum annealers with exact cover problems: Quantum Information Processing, **21**, 141.

Xavier, P. M., P. Ripper, T. Andrade, J. D. Garcia, and D. E. B. Neira, 2023, ToQUBO.jl.

Yulianti, L. P., and K. Surendro, 2022, Implementation of quantum annealing: A systematic review: IEEE Access, **10**, 73156–73177.